APPLICATION OF A VORTEX IDENTIFICATION METHOD FOR QUANTIFYING THE TIP LEAKAGE VORTEX WANDERING IN A LOW-SPEED AXIAL FAN CASE STUDY

B. Lendvai - T. Benedek

Department of Fluid Mechanics, Faculty of Mechanical Engineering, Budapest University of Technology and Economics, Bertalan Lajos u. 4 – 6., H-1111 Budapest, Hungary;
Email: lendvai.balint@gpk.bme.hu

ABSTRACT

The natural unsteadiness of turbomachinery tip leakage vortex has been reported in both measurement and simulation. The visualization and quantification of this vortex wandering are challenging using pathlines or simple vortex identification methods. In the present paper, the tip leakage vortex wandering is investigated in the case of a low-speed fan's unsteady Reynolds-averaged Navier-Stokes simulation. The wandering motion of the leakage vortex is detected by Banks' vorticity predictor – pressure corrector vortex core line localization method. Despite the low computational costs, the simulation predicted the complex vortical structure present in the blade passage. The vortex detection algorithm proved successful in finding the tip leakage vortex, but it failed to follow the core line upon heavy disturbance in the flow. The extent and the frequency of the vortex wandering were determined.

KEYWORDS: TIP LEAKAGE FLOW, VORTEX WANDERING, CFD, URANS, VORTEX CORE LOCALIZATION

NOMENCLATURE

Latin letters

n	rotor speed [RPM]	Δp_{t}	total pressure rise [Pa]
Q_v	volume flow rate [m^3/s]	r_t	tip radius [m]

Greek letters

Φ	flow coefficient [-]	ρ	fluid density [kg/m^3]
Ψ	total pressure coefficient. [-]		

INTRODUCTION AND OBJECTIVES

Low-speed axial flow fans are widespread both in industrial applications and in households as well. Therefore, high-efficiency and low noise-emission fans are in high demand. Still, one of the major sources of both losses and sound emission is the inevitable tip leakage flow which can cause up to nearly a third of the hydraulic losses of the fan and, in many cases, has been identified as the dominant sound source [1,2]. In the case of ducted axial flow fans, tip leakage flow rolls up and forms the tip leakage vortex (TLV). The onset of the TLV moves downstream along the chord as the fan is throttled, simultaneously, its swirling strength and the relative angle between the vortex trajectory and the blade tip chord line increase [3, 4]. The TLV trajectory has a significant influence over the flow in the blade passage: based on the fan geometry and the operation point, the tip leakage vortex either leaves the blade passage or impinges on the pressure side of the following blade [5]. By impinging on the following blade, the tip leakage vortex causes a large amount of blockage in the blade passage as well as interacts with the tip leakage flow of said blade; therefore, substantial additional losses are generated.

The unsteady behavior of the tip leakage vortex is well-documented in the case of axial flow turbomachines. This seemingly arbitrary motion of the vortex core around its temporarily averaged location is called vortex wandering. The vortex wandering phenomenon for the TLV has been shown with measurement [6, 7] and has been reproduced with simulation [8, 9] as well.

Jin et al. [6] experienced natural unsteady behavior of the TLV in PIV measurements. The vortex cores were identified by local vorticity maximum, the detected cores were randomly scattered in a circle. Lee et al [7] investigated the TLV wandering in a low-speed fan with PIV measurements. It was found that the magnitude of the vortex motion increases as the TLV travels downstream in the blade passage.

Boudet et al. [8] performed zonal large eddy simulations on an axial flow fan with a focus on the tip leakage flow. Natural unsteadiness was observed in the simulation based on coincident acoustic spectrum and velocity fluctuation. Thus, it was concluded that the TLV wandering was caused by either upstream casing induced turbulence instabilities or rotating instability.

A high-resolution large eddy simulation was carried out by Park et al. [9]. The TLV was found to be oscillating around the temporarily averaged vortex core location at a low frequency. The frequency of the oscillation could be identified based on the local axial velocity time series. The motion of the TLV was mainly in the azimuthal direction. Locally increased turbulent kinetic energy, which promotes losses, around the vortex core was reported by both Park et al and Lee et al which was due to the natural unsteadiness.

Flow visualization is challenging during the examination of the tip leakage vortex. In both measurement and numerical simulation results, the tip vortex is mainly represented by streamlines or a simple vortex identification method such as the λ_2 [10] and the Q criterion [11]. However, these commonly used flow visualization techniques are for vortex region detection, and they are not able to determine the location of the core, i.e., the position of the vortex. Thus, these methods are sufficient for qualitative findings, but quantitative results cannot be filtered out. In contrast to flow visualization methods, vortex core detection methods are able to track the motion of the vortex core; thus, the change in the vortex location over time can also be quantified [12].

The most straightforward vortex core line detection technique would be to look for local line type extrema of quantities associated with vortex cores such as pressure minima and vorticity maxima. Thus, ridge line detection methods could be implemented for vortex core detection, such as the pressure valley detection of Miura and Kida [13]. However, these ridge detection algorithms require higher order derivatives of said quantities which are computationally costly to calculate as well as extremely fine mesh resolution is necessary for high accuracy. Also, it is suggested that these quantities in themselves are not capable of describing the vortex skeleton since both pressure and vorticity are drastically affected by the flow features [12]. For instance, solid surfaces submerged in fluid flows produce vorticity and pressure deviations comparable to if not stronger than the vortex itself.

A different approach was presented by Jiang et al. [14]. It was suggested to look for locations where the velocity field of the neighboring cells describes a closed loop. This step narrows down the potential locations of the vortices then a computationally more costly local vortex identification method is carried out at the previously marked locations. The method is easily applicable for 2D cases, however, in the case of 3D simulations choosing the plane perpendicular to the vortex core in which the velocity field shall be evaluated is not straightforward.

In the case of strongly curved vortices, a higher-order vortex identification method is required, such as the method proposed by Roth and Peikert [15] for the detection of the vortex line. The

technique assumes bent vortices with zero-torsion. With this presumption, the vortex core line is defined as the set of points where the local velocity is parallel to its second total derivative.

Ridgeline detection algorithms [13] and the higher order vortex identification method [15] require second spatial and total derivatives respectively which introduce significant uncertainties in the case of computational fluid dynamics evaluations. The effect is amplified for skewed and irregular numerical grids typical for swept and skewed turbomachines.

In the present case study, the blade tip vortex wandering of a low-speed axial flow fan will be investigated with an unsteady Reynolds-averaged Navier-Stokes (URANS) simulation. Complementing this and supporting the processing of the results, Banks' vorticity predictor – pressure corrector vortex core identification method [16] was implemented. The technique uses predefined seed points to grow the vortex skeleton. Starting from a seed point, the vortex detection algorithm in the first step predicts the vortex core direction based on the local vorticity vector. Following this, the prediction is corrected by searching for nearby pressure minimum.

Unlike the ridge line and the higher order methods, Bank's vorticity predictor–pressure corrector technique does not rely on numerical derivatives and the vortex skeleton is calculated based on local field variables only. Vinha et al. [17] successfully applied the Banks' method for the URANS simulation of a counter-rotating open rotor (CROR) engine. The resulting vortex skeletons showed agreement with both the λ_2 [10] and the Q criterion [11]. As highlighted by Vinha the drawback of Banks' method is its sensitivity to seed positions.

Using a vortex skeleton detection algorithm, the instantaneous vortex trajectory can be determined. Employing the process at different time instances the extent of the vortex core wandering can be established. The method developed and applied in the case study can be generalized and employed for cases where the fan is operated near the limit of the TLV impinging on the following blade, where methods for preventing the impingement can be developed.

FAN OF CASE STUDY, METHODOLOGY

The investigated low-speed axial flow fan of the case study has five forward-skewed controlled vortex design blades with circular arch profiles. The radii of the blade tips were r_b = 0.15 meters with a 0.3 tip-to-hub ratio. The blade tip gap was set to 5% of the blade tip radius. Detailed geometric data on the blades of the fan are documented in Benedek and Vad [18]. The characteristic curves of the fan in a ducted arrangement can be found in [19].

The fan was operating at $n = 1400\ RPM$ for the simulation. This corresponds to the mid-chord based Reynolds number of 105 000. The fan was investigated at the global flow coefficient $\Phi = 0.28$, which is a somewhat lower flow rate than the peak efficiency operating point $\left(\Phi_{maxeff} = 0.3\right)$. The corresponding total pressure coefficient was $\psi_{tot} = 0.198$. The flow and pressure coefficients were calculated using Eq. 1-2.

$$\Phi = \frac{Q_V}{r_b^3 \cdot \frac{n}{60} \cdot \pi^2 \cdot 2} \tag{1}$$

$$\psi_{tot} = \frac{\Delta p_{\mathrm{t}}}{\rho \cdot r_b^2 \cdot \left(\frac{n}{60}\right)^2 \cdot \pi^2 \cdot 2} \tag{2}$$

The unsteady Reynolds-averaged Navier-Stokes (URANS) numerical simulation was carried out in ANSYS Fluent 21R1 software. The turbulence effects were modeled with the k-ω shear stress transport turbulence model [20]. Using the circumferential periodicity of the fan rotor, only a single

blade passage was modeled with rotationally periodic boundaries. For the simulations, the frozen rotor approach was used with a prescribed rotating frame of reference for the zone containing the rotor while the inlet and outlet ducts had a stationary frame of reference. The simulation domain is shown in Fig. 1.

In the simulations 3 r_b long inlet duct section was employed with velocity inlet. The specified velocity, turbulent kinetic energy, and specific turbulent dissipation rate distributions were previously calculated using a fully developed periodic duct simulation. The free exhaust surface was set as constant static pressure outlet at the end of the 10 r_b long outlet duct, thus, neither boundary conditions had any effect on the fan operation.

The unsteady simulations were initialized with 50 blade passes which was assumed to be enough for the vortex wandering to develop. Afterward, the data sampling was started for an additional 10 blade passes. The timestep was set as 5e-6 seconds with second order implicit time integration scheme. This time step size satisfies the cell convective Courant number condition. The data acquisition was initialized every 5e-4 seconds.

Since the aim of the case study was to establish a method for investigating the vortex wandering of the TLV, only the blade tip region of the mesh was well-refined. Further from the blade tip a coarser mesh was prescribed. A structured O-grid mesh with around 1 million hexahedral cells was prepared for the rotor. The blade was meshed with 75 and 60 cells in the streamwise and radial directions respectively with more refined mesh near the blade leading edge, trailing edge, and especially towards the blade tip. The domain was modeled into 120 cells circumferentially. The blade thickness was resolved with 20 cells, while the tip gap was divided with 25 cells radially. The H-grid duct meshes contained 150 000 cells with high-resolution boundary layer meshes. Mesh sensitivity analysis was carried out through isotropic mesh adaptation. The resulting numerical mesh containing close to 9 million cells showed similar results to the used mesh with respect to the operating point (below 0.6% difference), and efficiency (below 0.5% difference), while the vortex wandering location, amplitude, and frequency were identical for the two meshes. Thus, the used mesh was considered adequate. The numerical mesh can be seen in Fig. 2.

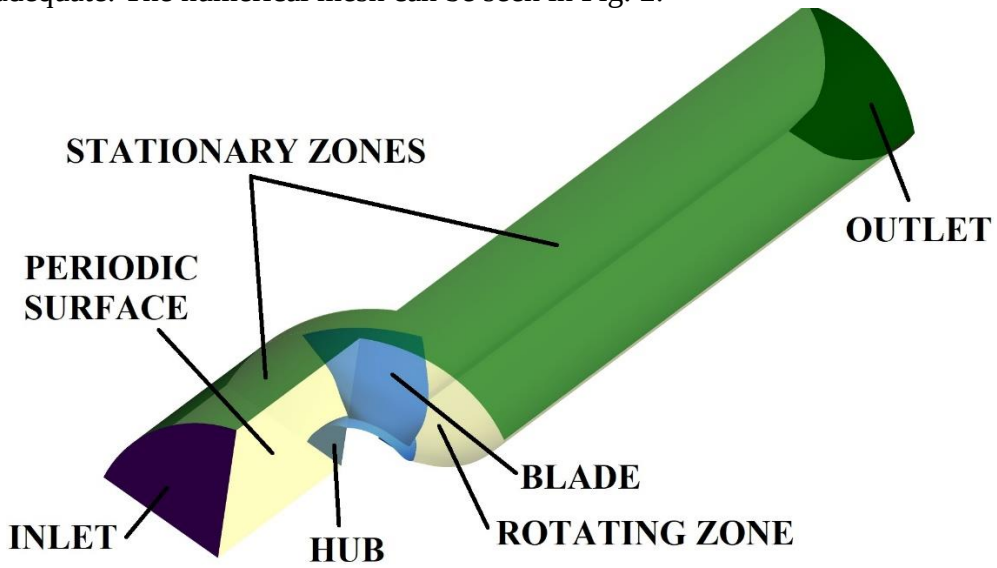

Figure 1: Simulation domain.

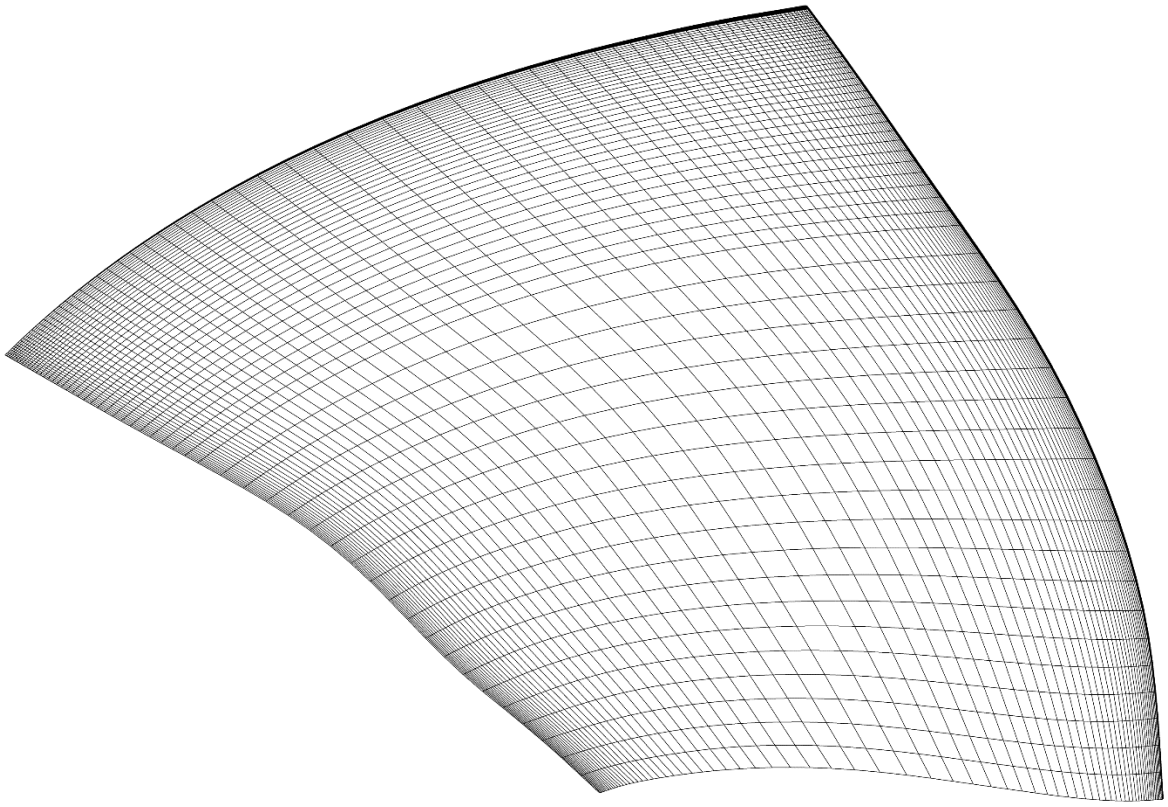

Figure 2: The structured mesh of the simulations.

A preliminary study was carried out on an elbow duct with converging upstream and diverging downstream duct sections with prescribed swirling inflow. Even though the mesh of the preliminary study was significantly less skewed and more uniform than the one used for the fan simulation the numerical derivatives showed considerable errors. On the other hand, Banks' vorticity predictor – pressure corrector vortex core line detection technique [16] was found to be accurate, robust, and independent of mesh quality, thus, it was found to be the most suitable for the application. The used method is also favorable as it has extremely low computational costs compared to the higher-order ridge detection algorithms. The implemented vortex core identification is completed for a time instance in a minute on a single CPU core (AMD Ryzen 5 5625U) with the used input parameters.

Banks' vortex core identification technique follows vortex skeletons from predefined seed points in two steps. Firstly, the following point in the vortex core is predicted with the vorticity vector. However, it is well-known that the vorticity vector may not align with the vortex core, thus, integrating along the vorticity vector does not follow the vortex skeleton. Therefore, in the corrector step, the pressure minimum corresponding to the vortex core is sought in the plane perpendicular to the vorticity vector at the predicted point. Likewise to the vorticity integral, a set of pressure minimum points do not automatically constitute a vortex core line as external flow features also affect the pressure distribution. However, with the combination of the predictor and corrector steps, the vortex skeleton is likely to be entirely identified.

The predictor-corrector method also has multiple tunable input parameters. The initial step size determines the resolution of the vortex skeleton. It was found that 0.4% of the chord length step size proved adequate for the used mesh resolution. In the corrector step, the pressure minimum was sought on a 0.08% chord length by 0.08% chord length surface perpendicular to the vorticity of the predicted

point. The ratio of step size and corrector surface edge length determine the maximum angular deviation between the vorticity and the vortex core line. With the given parameters the maximum deviation was set as 11.3 degrees.

The hardest part of the algorithm is finding adequate seed positions for the vortex skeleton to develop from. Banks suggests locating seeds with local pressure minima and vorticity maxima. However, near the blade tip leading edge, where the TLV originates, local separations and the solid wall disturbs the pressure and vorticity distributions, making seed localization impossible. For this reason, the seed was located somewhat downstream of the blade leading edge using pressure minimum and vorticity maximum locations. This way, finding seeds is easily attainable, and reversing the technique allows the tracking of vortex skeletons in a reverse direction. The vortex skeletons were terminated at the interface surface between the rotating zone and the outlet duct.

The simulation data were extracted at each cell center and a hypersurface was interpolated for the whole investigated domain. Between the mesh cell centers, the natural neighbor interpolation method was used which made the resulting vortex line somewhat noisy. A smoother resolution could have been attainable with a finer mesh. The periodic domain was also accounted for in the postprocessing of the data.

RESULTS

Firstly, the developed flow field and vortical structures in the blade passage are investigated. Figure 3. shows the vortex regions displayed by the Q criterion. The main TLV originates close downstream of the blade tip leading edge, and it dominates the flow field. A major secondary tip leakage vortex is highlighted in the figure which is located at 70% chord. Postprocessing the simulation data revealed that a low axial velocity annular fluid region develops around the downstream half of the blade tip chord length, thus, creating and maintaining double leakage and multi-leakage flow. The stagnating fluid rolls up into the vortex close upstream of the trailing edge and travels in the circumferential direction towards the following blade until it collides with the main TLV at 70% chord. The impingement of vortices increases mixing and promotes turbulent kinetic energy production. The extreme level of multi-leakage flow is caused by the investigated operating point and the relatively high tip gap size.

Besides the tip leakage vortices, an induced vortex with an opposite rotational direction to the main TLV is visualized upstream of and parallel to the TLV which matches the results of Decaix et al [21]. The figure also shows a slight discontinuity in the isosurfaces at the rotational periodic boundary caused by the non-conformal grid interface. All three major vortices and the stagnating zone are displayed in Figure 3.

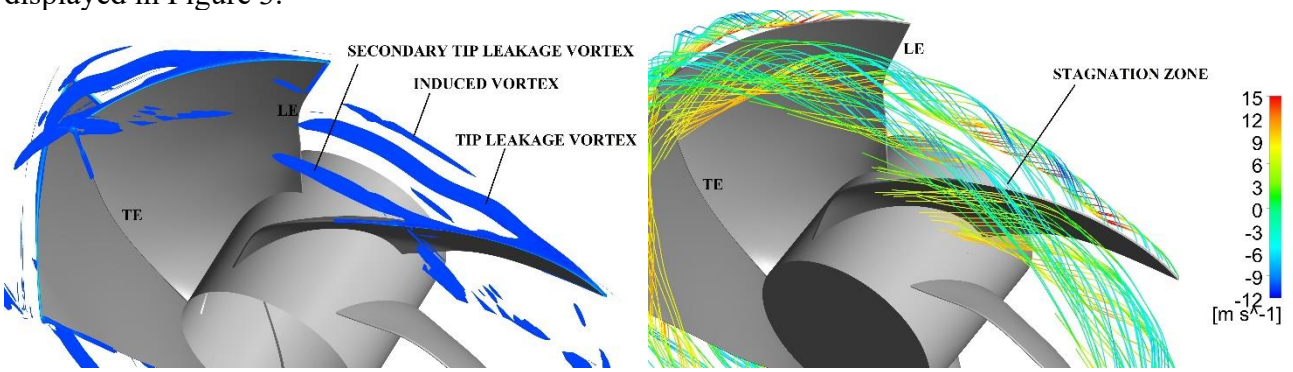

Figure 3: The dominant vortical structure of the developed flow field inside the blade passage. Left: Q criterion, Q = 2e6. Right: streamlines started from the blade tip colored by the axial velocity. LE = leading edge, TE = trailing edge.

Secondly, the vortex identification capabilities of the implemented predictor-corrector vortex core detection algorithm will be analyzed. Given that the aim of the case study was to determine the extent of the TLV wandering, in the forthcoming only the main TLV and its unsteady behavior will be investigated. Therefore, only the single most prominent seed was chosen in the seeding process for all time steps.

Postprocessing the results showed the advantages and the disadvantages of the applied vortex core detection algorithm. On one hand, the simulation data would be challenging for any vortex core detection method as the developed vortex structure contains multiple vortices colliding. Unfortunately, the implemented vorticity predictor–pressure corrector vortex localization algorithm fails to track the vortex core line beyond the vortex collision. On the other hand, the method is perfectly capable of determining the vortex core line of the TLV up until 70% chord. The method shows ideal results with multiple vortex region detection methods, the calculated vortex core line, and Q-criterion isosurfaces can be seen in Figure 4. Thus, from here on the vortex cores are sliced at 60% chord in order to focus on the main TLV wandering. The seeding of the main TLV was fruitful as local pressure minima and vorticity maxima proved effective in finding the main TLV for arbitrary axial locations. Also, different seeding positions resulted in similar vortex core lines and the algorithm indeed works in the reverse direction as well.

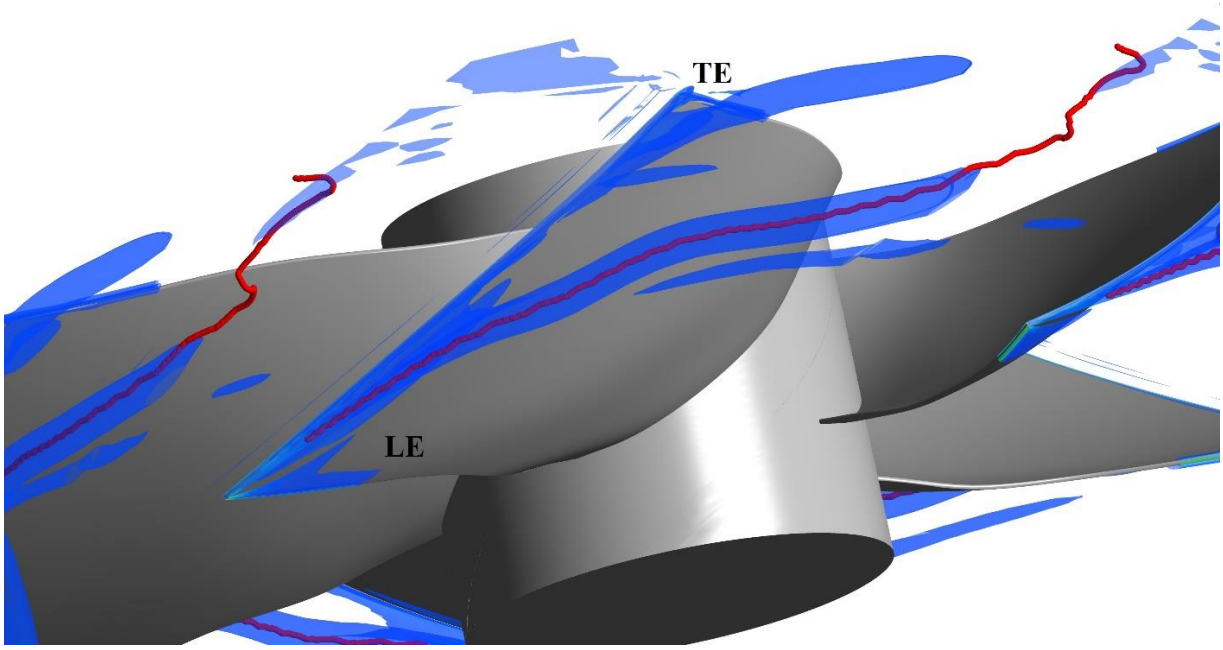

Figure 4: The vortex core line calculated by the predictor-corrector method and Q-criterion isosurfaces, Q = 2e6. LE = leading edge, TE = trailing edge.

Also, the parameter sensitivity of the algorithm was investigated. Increasing the predictor step size lowered the resolution of the results, yet the method still successfully identified the TLV and its core even in the case of 4% chord length step size. The effect of the corrector area size was also examined. It was found that the detected TLV core was unaffected by corrector area size as well. However, the parameter had a significant influence on the latter part of the core line: the core line was diverted towards the casing by the mixing of the vortices for relatively small corrector area sizes. Nevertheless, increasing the corrector area size, thus increasing the maximum allowed angle between

the vorticity vector and the pressure minimum line, resulted in following a vortex core line that passed across the tip gap of the following blade and then left the blade passage.

Finally, the extent of vortex wandering was determined from the simulation results. The vortex core line was segmented at predefined axial locations corresponding to 17%, 25%, 33%, 42%, and 50% chord. A plane was set perpendicular to the local vorticity vector at one of the investigated time instances. Then, each TLV core line was linearly interpolated onto the section plane. The section planes and the vortex cores for the investigated time instances are depicted in Figure 5.

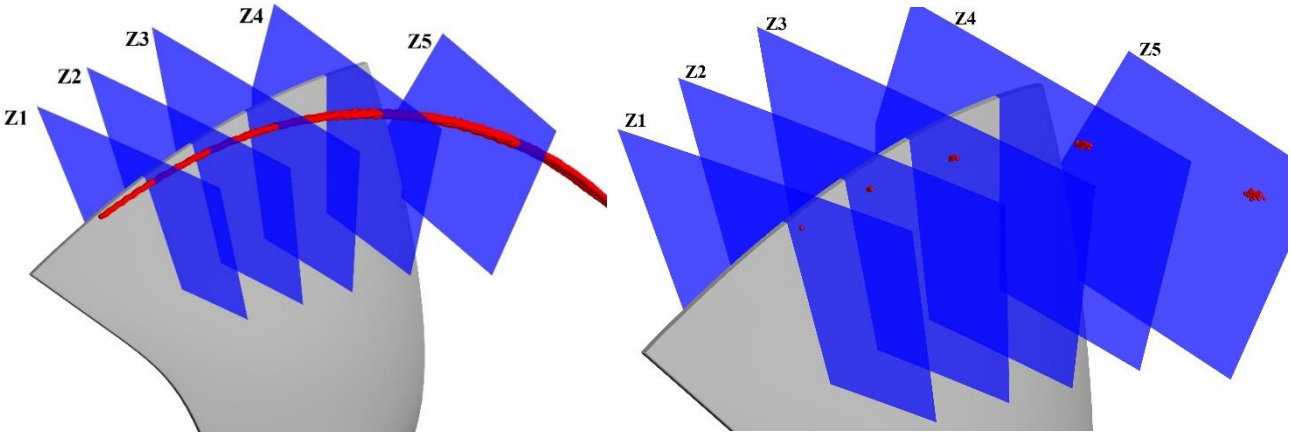

Figure 5: The vortex core lines and their section points at the section planes in the blade passage for all investigated time instances.

The scatter plots of vortex cores show an ellipsoid shape on the section planes. Connecting the individual vortex core locations on the section planes in chronological order displays the quasi-periodic motion of the vortex core at the section plane. The vortex path for several periods can be seen in Figure 6. for the planes corresponding to 33% (plane Z3) and 50% (plane Z5) chords. The extent of the vortex wandering was nondimensionalized with the tip chord length. The pattern reveals that the vortex moves around on an elliptical path quasi-periodically with the dominant frequency being 6 samplings per period. This corresponds to roughly 300 Hz frequency. Based on measurement and simulation the first 10 natural frequencies of the investigated fan are between 100 and 200 Hz [22]. Therefore, in the case of the vortex wandering frequency scales with the blade tip velocity then a lower rotational speed may induce vibrations as well.

The frequency of the vortex wandering can also be expressed with the nondimensional frequency called the Strouhal number. However, the method of nondimensionalizing the frequency is equivocal. Park et al [9] calculated the Strouhal number to be 1.0 based on blade tip radius and blade tip velocity. Their definition is unfavorable as it suggests that the vortex wandering frequency is independent of the operating point of the turbomachine. On the other hand, Boudet et al [8] computed the Strouhal number of the vortex wandering to be 1.0 based on relative streamwise velocity at the blade tip and blade tip chord length. This definition is more suitable as the tip leakage vortex phenomenon is directly influenced by the local velocity and geometric features. It is clear that the Strouhal number definitions listed above are not equivalent, the numerical value being identical is merely a coincidence. Also, Jin et al [6] reported natural unsteadiness over a wider frequency range, thus, a unique Strouhal number is not straightforward.

Applying the Strouhal number definition of Park and Boudet for the results of the case study gives the Strouhal numbers 2.05 and 2.20 respectively.

The vortex wandering was also quantified for all investigated section planes. The maximum distance between cores at the section planes nondimensionalized with the tip chord length can be found in Table 1. The magnitude of the vortex wandering grew continuously along the path of the vortex core. Also, Jin et al [6] reported tip leakage vortex core location displacement of 6.4% of the blade tip chord length at 50% chord length on a plane perpendicular to the chord line.

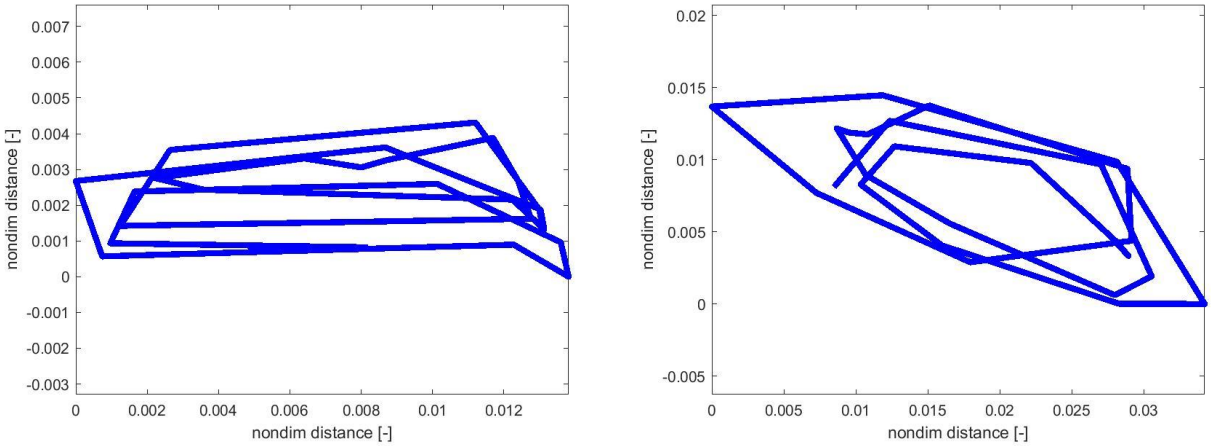

Figure 6: Vortex core paths at planes Z3 and Z5 corresponding to 33% chord axial locations (left) and 50% chord axial locations (right).

Table 1: Vortex wandering maximum displacement nondimensionalized by the tip chord length at investigated section planes.

plane number	Z1	Z2	Z3	Z4	Z5
plane location	17% chord	25% chord	33% chord	42% chord	50% chord
nondimensionalized vortex wandering maximum distance	1.69e-3	7.43e-3	1.49e-2	2.92e-2	3.83e-2

CONCLUSIONS

In the present paper, the tip leakage vortex wandering of a low-speed axial flow fan was investigated. The unsteady behavior of the tip leakage flow was simulated with an unsteady Reynolds-averaged Navier-Stokes simulation. Banks' vorticity predictor-pressure corrector vortex core detection method was implemented for tracking the transient motion of the vortex.

A rather complex vortical structure developed in the blade passage as a secondary tip leakage vortex caused by multi-leakage flow appeared. The main tip leakage vortex (TLV) originated from the 5% chord of the blade tip. The secondary tip leakage vortex originating from the trailing edge migrated circumferentially until it collided with the main TLV. The vortex core detection method successfully localized and followed the main TLV until the vortices collided, where it diverged. The algorithm showed little dependency on the method parameters and the seeding process.

Finally, the extent of vortex wandering was determined. The vortex core line was sectioned by five planes perpendicular to its tangential. The extent of the vortex wandering was calculated at these planes, and it showed a continuously increasing trend in the flow direction moving away from the

leading edge. The results showed that the motion of the main TLV is quasi-periodic, with a dominant frequency of ~300 Hz.

ACKNOWLEDGEMENTS

Supported by the ÚNKP-22-3-I-BME-90 New National Excellence Program of the Ministry for Culture and Innovation from the source of the National Research, Development, and Innovation Fund. This work has been supported by the Hungarian National Research, Development, and Innovation Fund under contract NKFI K 129023.

REFERENCES

[1] Longhouse R. (1978) Control of tip-vortex noise of axial flow fans by rotating shrouds. Journal of Sound and Vibration 58(2): 201–14. doi:10.1016/S0022-460X(78) 80075-3.
[2] Fukano T, Jang C-M. (2004) Tip clearance noise of axial flow fans operating at design and off-design condition. Journal of Sound and Vibration 275(3):1027–50. doi:10.1016/S0022-460X(03)00815-0.
[3] Jang, C., Sato, D., Fukano, T. (2004) Experimental Analysis on Tip Leakage and Wake Flow in an Axial Flow Fan According to Flow Rates. ASME. Journal of Fluids Engineering 127(2): 322–329. doi:10.1115/1.1881695
[4] Zhang, D., Shi, W., van Esch, B.P.M., Shi, L., Dubuisson, M. (2015) Numerical and experimental investigation of tip leakage vortex trajectory and dynamics in an axial flow pump. Computers & Fluids, Volume 112, Pages 61-71, ISSN 0045-7930, doi: 10.1016/j.compfluid.2015.01.010
[5] Benedek, T., Lendvai, B., Vad, J. (2022) Combined acoustic and aerodynamic investigation of the effect of inlet geometry on tip leakage flow noise of free-inlet free-exhaust low-speed axial flow fans. Applied Acoustics, 187 (2022) 108488 doi:10.1016/j.apacoust.2021.108488
[6] Jin, G.-Y., Ouyang, H., Wu, Y.-D., Du, Z.-H. (2011) An experimental study of the unsteady characteristics of tip-leakage flow of axial fans with circumferential skewed blades at off-design conditions. Proceedings of the Institution of Mechanical Engineers, Part A: Journal of Power and Energy. 225(6):802-816. doi:10.1177/0957650911404621
[7] Lee, H., Park, K., Choi, H. (2019) Experimental investigation of tip-leakage flow in an axial flow fan at various flow rates. Journal of Mechanical Science and Technology **33**, 1271–1278 doi: 10.1007/s12206-019-0227-z
[8] Boudet, J., Cahuzac, A., Kausche, P., Jacob, M. C. (2015) Zonal Large-Eddy Simulation of a Fan Tip-Clearance Flow, With Evidence of Vortex Wandering. ASME. Journal of Turbomachinery 137(6): 061001. doi:10.1115/1.4028668
[9] Park, K., Choi, H., Choi, S., Sa, Y.C., & Kwon, O. (2017) Unsteady Characteristics of Tip-Leakage Flow in an Axial Flow Fan. Proceeding of Tenth International Symposium on Turbulence and Shear Flow Phenomena.
[10] Jeong, J., Hussain, F. (1995) On the identification of a vortex. Journal of Fluid Mechanics, 285, 69-94. doi:10.1017/S0022112095000462
[11] Hunt, J., Wray, A., Moin, P. (1988) Eddies, streams, and convergence zones in turbulent flows. Studying Turbulence Using Numerical Simulation Databases. -1. 193-208.
[12] Epps, B. (2017) Review of Vortex Identification Methods. 55th AIAA Aerospace Sciences Meeting. doi:10.2514/6.2017-0989
[13] Miura, H., Kida, S. (1997) Identification of Tubular Vortices in Turbulence. Journal of the Physical Society of Japan 66(5), 1331–1334. doi:10.1143/jpsj.66.1331

[14] Jiang, M., Machiraju, R., Thompson, D. (2002) A Novel Approach to Vortex Core Region Detection. Proc. of VisSym '02. 217-ff.
[15] Roth, M., Peikert, R. (1998) A Higher-Order Method for Finding Vortex Core Lines. Proc. Visualization '98. 143-150. doi:10.1109/VISUAL.1998.745296.
[16] Banks, D. C., Singer, B. A. (1995) A predictor-corrector technique for visualizing unsteady flow. IEEE Transactions on Visualization and Computer Graphics 1(2), 151–163. doi:10.1109/2945.468404
[17] Vinha, N., Vallespin, D., Valero, E., de Pablo, V., Cuesta-Lopez, S. (2020) Numerical prediction of vortex trajectories and vortex–blade interaction on the CROR engine. Aircraft Engineering and Aerospace Technology, Vol. 92 No. 9, pp. 1345-1356. doi:10.1108/AEAT-03-2020-0044
[18] Benedek, T., Vad, J. (2014) Concerted aerodynamic and acoustic diagnostics of an axial flow industrial fan, involving the phased array microphone technique. ASME Paper GT2014-25916
[19] Lendvai, B., Benedek, T. (2022) Study on the effect of sudden duct diameter change on the performance of an axial flow fan. Conference on Modelling Fluid Flows 2022 (CMFF'22)
[20] Menter, F. R., (1993) Zonal Two Equation k-ω Turbulence Models for Aerodynamic Flows. 23rd Fluid Dynamics, Plasmadynamics, and Laser Conference
[21] Decaix, J., Balarac, G., Dreyer, M., Farhat, M., Münch, C. (2015) RANS and LES computations of the tip-leakage vortex for different gap widths. Journal of Turbulence 16:4, 309-341, doi: 10.1080/14685248.2014.984068
[22] Kalmár-Nagy, T., Bak, B. D., Benedek, T., Vad, J. (2015) Vibration and Noise of an Axial Flow Fan. Periodica Polytechnica Mechanical Engineering 59(3), pp. 109–113, doi:10.3311/PPme.7948

